Available online at www.sciencedirect.com
SCIENCE DIRECT®
ELSEVIER
Nuclear Instruments and Methods in Physics Research B 241 (2005) 118–124
NIM B
Beam Interactions with Materials & Atoms
www.elsevier.com/locate/nimb

Laser photodetachment electron spectroscopy studies of heavy atomic anions

Vernon T. Davis [a,*], Jeffery Thompson [b], Aaron Covington [b]

[a] United States Military Academy, P.O. Box 93, West Point, NY 10996, United States
[b] University of Nevada, Reno MS 220, Reno, NV 89557-0058, United States

Available online 18 August 2005

Abstract

Laser photodetachment electron spectroscopy (LPES) experiments have been performed at the Negative Ion Research Facility at the University of Nevada, Reno, using a crossed ion-laser beams apparatus to investigate the structure and dynamics of heavy atomic anions. A small ion accelerator is used to produce monoenergetic beams of negatively-charged atomic ions. Ejected electrons (photoelectrons), produced by the collision of the ions with linearly-polarized photons, are collected and their kinetic energy is measured with a hemispherical-sector electrostatic analyzer. The resultant photoelectron spectrum is used to determine the electron affinity (EA) of several of the lanthanides, while limits on the electron affinities for others are inferred. In addition, the angular asymmetry parameters and angular distribution patterns of photoelectrons created by laser photodetachment of several heavy atomic anions, as well as the spectral dependence of those angular distributions, have been determined. Electron affinities and photoelectron angular distribution asymmetry parameters can offer crucial information regarding the electronic structures of these heavy atomic anions, and represent key information for models of these complex systems.

PACS: 32.80.Gc; 32.10.Hq; 32.10.−f; 33.60.−q

Keywords: Electron affinity; Negative ions; Lanthanides; Hafnium

Negative ions continue to be the subject of intense theoretical and experimental interest, as the structure of a negative ion is fundamentally different from that of a neutral atom or positive ion due to an increased screening of the nuclear charge [1]. The masking of the nuclear-electron interaction in negative ions increases the relative significance of short-range electron–electron forces that allow for only a limited number of bound

* Corresponding author. Tel.: +1 435 831 7260; fax: +1 435 831 7252.
E-mail addresses: vernon.davis@us.army.mil, vernon.davis@usma.edu (V.T. Davis).

0168-583X/$ - see front matter
doi:10.1016/j.nimb.2005.07.073

states, and the resultant short-range potential is responsible for the relatively small binding energies of stable atomic negative ions.

The formation of negative ions depends on the subtleties of the dynamics of the electron–electron interactions to provide a potential sufficient to bind an extra electron to a neutral system. Sophisticated calculations, which account in detail for electron correlation, are employed for investigating even simple atomic negative ions. Approximation schemes are typically used to reduce the number of terms included in the calculations so that numerical techniques may be successfully employed. Several reviews of negative ion research [2–5] have pointed out the computational complexity encountered by theoretical investigations of lanthanide and other heavy atomic anions and the limited number of experimentally measured results for these ions. Experimental verification of the existence of predicted negative ion structures and binding energies is therefore important for validating approaches used in theoretical calculations.

Semi-empirical estimates of the electron affinities of certain lanthanides and hafnium have been reported [6–8]. Recent calculations, reported by a number of authors using several different computational techniques, predict the formation of stable negative lanthanide ions by the attachment of a 6p electron [9–17], (although this is disputed for Tm [18]) rather than a 4f electron. Also, a recent article investigates the attachment of 5d and 6p electrons to cerium [19]. Previous experimental investigators have reported production of stable lanthanide negative ions and hafnium using accelerator mass spectrometry techniques [20,21]. All of the lanthanide negative ions were observed except Pm^-, Ho^- and Er^- [20]. The reported negative ion production yields for La^- and Ce^- were much higher than those of the other atomic lanthanides, indicating that either the electron affinities of lanthanum and cerium are greater than the EAs of other rare-earth atoms, or La^- and Ce^- have more than one bound state [20,21]. Subsequent LPES studies of these two species indicate that La^- and Ce^- do have multiple bound states, but their EAs are actually lower than those of some other lanthanides (see Table 1). The relative yields of sputtered negative ions were used by Nadeau et al. to compare binding energies, but only as an indication of relative values. Using this technique, Nadeau et al. have reported lower limits on the EAs for the lanthanides and hafnium [21].

LPES techniques can also be used to measure the distributions of ejected photoelectrons. Photoelectron angular distribution asymmetry parameters can offer crucial information about the electronic structures of heavy atomic anions, since, if the results of such measurements confirm to certain models, predominant contributions to valence-electron structure can be inferred.

The most general form of the angular distribution of a collision process for an unpolarized target was summarized by Yang [22]. Cooper and Zare [23,24] developed a form of the differential cross section for the production of photoelectrons detached from a randomly polarized target by linearly polarized incident light. The differential cross section can be written in the dipole approximation as

$$\frac{d\sigma}{d\Omega} = \frac{\sigma}{4\pi}\left[1 + \frac{\beta}{2}(3\cos^2\theta - 1)\right], \tag{1}$$

where σ is the total photodetachment cross section at a given photon energy, θ is the angle between the polarization vector of the photon and the momentum vector of the photodetached electron, and β is the asymmetry parameter, which completely characterizes the shape of the photoelectron emission pattern. The differential cross section must be nonnegative, which restricts the range of the asymmetry parameter to $-1 \leqslant \beta \leqslant 2$. Within the independent-particle approximation, the asymmetry parameter for the photo-ejection of an electron from an unpolarized initial state with angular momentum l, is given by

$$\beta = \frac{l(l-1)R_{l-1}^2 + (l+1)(l+2)R_{l+1}^2 - 6l(l+1)R_{l+1}R_{l-1}\cos(\delta_{l+1} - \delta_{l-1})}{(2l+1)\left[lR_{l-1}^2 + (l+1)R_{l+1}^2\right]}. \tag{2}$$

The asymmetry parameter is found to be most sensitive to the phase-shift differences $\delta_{l+1} - \delta_{l-1}$, though it also depends on the relative magnitudes of the radial matrix elements R_{l+1} and R_{l-1}. Cooper and Zare [23] also showed that Eq. (2) is valid for LS coupling.

Table 1
EAs of heavy elements measured in this study are compared to the results of other recent studies

Element	Ground state	LPES	Other studies (method)
La	$^2D_{3/2}$	0.470(20) [32]	>0.5 (AMS) [21] 0.27-0.41 (DFT) [10] 0.33 (RCCSD) [31]
Ce	$^1G^0_4$	0.955(26) [33]	0.428 (MCDF-RCI) [17] >0.5 (AMS) [21] 0.7 (AMS) [34]
Pr	$^4I^0_{9/2}$	0.926(24) [35]	0.128 (MCDF-RCI) [36] >0.1 (AMS) [21]
Nd	$^5I_4$	>1.916	>0.05 (AMS) [21]
Pm	$^6H^0_{5/2}$	Not studied	
Sm	$^7F_0$		>0.05 (AMS) [21]
Eu	$^8S^0_{7/2}$	1.053(25) [37]	>0.05 (AMS) [21]
Gd	$^9D^0_2$		>0.1 (AMS) [21]
Tb	$^6H^0_{15/2}$	>1.165	>0.1 (AMS) [21]
Dy	$^5I_8$	>0	0.015(3) (EFD) [21]
Ho	$^4I^0_{15/2}$		<0.005 (EFD) [21]
Er	$^3H_6$		<0.005 (EFD) [21]
Tm	$^2F^0_{7/2}$	1.029(22) [38]	0.027-0.136 (DHF-DFT) [15] 0.032(7) (EFD) [21]
Yb	$^1S_0$	Not bound	Detected (EFD) [39] 0.054(27) (DFT) [9] 0.0985 (CI) [11] 0.001 (DHF) [40] <0.003 (LPRI) [41]
Lu	$^2D_{3/2}$	0.346(14) [42]	0.190(110) (DHF-DFT) [12] 0.257 (RCCSD) [16] >0.1 (AMS) [21]
Hf	$^3F_2$	>0	>0.1 (AMS) [21]

LPES = Laser photoelectron spectroscopy; MCDF-RCI = Multiconfigurational Dirac–Fock-relativistic configuration interaction; EFD = Electric field disassociation; AMS = Accelerator mass spectroscopy; DHF-DFT = Dirac–Hartree–Fock-density functional theory; DFT = Density functional theory; CI = Configuration interaction; DHF = Dirac–Hartree–Fock theory; LPRI = Laser photodetachment resonant ionization; RCCSD = Relativistic coupled cluster theory with single and double excitation. All EAs are given in eV.

Hanstorp et al. [25], using assumptions based on threshold behavior, developed a straightforward simplification of the Cooper–Zare model of the asymmetry parameter for photodetachment of p-orbital electrons,

$$\beta(\varepsilon) = \frac{2A_2\varepsilon(A_2\varepsilon - 2c)}{1 + 2A_2^2\varepsilon^2}. \quad (3)$$

In this formula, ε is the photoelectron energy and A_2 corresponds to the relative size of the two radial matrix elements, R_2/R_0, under the assumption that there is no residual interaction between the photoelectron and the residual neutral, and c is substituted in Eq. (2) for the cosine of the differences in the phase shifts, $\cos(\delta_2 - \delta_0)$. This equation predicts the correct spectral dependence for the asymmetry parameter β for photodetaching a p-orbital electron. The asymmetry parameter is zero at threshold due to the dominance of s-wave photoelectrons, decreases to a minimum value when $\frac{\sigma_2}{\sigma_0} = 0.5$, and approaches a value of $\beta = 1$ at large photoelectron energies.

The first detailed experimental study of angular distributions of photodetached electrons was

conducted by Hall and Siegel [26]. Subsequent measurements of angular distributions have been reported, but relatively few experiments have been conducted to investigate the energy dependence of photoelectron angular distributions for negative ions [25–27, and references contained therein].

A detailed description of the LPES experiment has been given elsewhere so only a brief description is presented [28]. The experimental apparatus consists of a commercial cesium-sputter ion source, ion beam transport system and optics, and an interaction chamber in which photoelectrons were produced in a crossed laser-ion beams geometry (see Fig. 1). Negative ions produced in the sputter source, after acceleration and extraction, were momentum-selected by a 90° bending magnet. The selected species was then steered and focused into the interaction chamber, where photodetachment of the negative ions was accomplished by a monochromatic cw laser beam crossing the ion beam at an angle of 90°. The photon beam was produced by cw lasers operating at several different wavelengths and delivering between 0.3 and 10 W to the interaction chamber. Copper dimer anions $^{A}Cu_2^-$ ($A = 126, 130$) produced from sputtering of copper powder were used as mass markers to identify the appropriate ion beams. Typical ion beam currents, as measured in a shielded Faraday cup in the interaction chamber, ranged from 70 pA to 1 nA.

Photoelectrons produced in the interaction region with the correct trajectory fell into the acceptance cone of 160° spherical sector spectrometer located at an angle of 45° beneath the plane defined by the ion and laser beams, and operating at a constant pass energy. Electrons with the correct kinetic energy passed through the analyzer and were detected by a channel electron multiplier. Phototelectron spectra were then generated by linearly decreasing the accelerating potential across the analyzer entrance. Both the laser beam power and ion beam current were measured to ensure proper normalization of photoelectron yields. Photoelectron angular distribution information was collected by rotating the polarization vector of the laser photons as they enter the interaction chamber with a double Fresnel Rhomb polarization rotator, and recording the total photoelectron yield at each angle.

The EA for several of the lanthanides and hafnium was determined using the LPES method. As an example, a typical photoelectron kinetic energy spectrum for Lu^- is shown in Fig. 2. The energy scale and transition width for the Lu^- photoelectron kinetic energy spectra were fixed using fine-structure-resolved reference photoelectron energy spectra of Na^- taken in conjunction with the Lu^- scans, and the known EA of Na [4].

After the Lu^- photodetachment spectra were transformed into the ion rest frame, the spectra were interpreted using spectroscopic data for the lutetium atom [29]. The energy separation of the photoelectron peaks corresponds to the initial and final states for the process,

$$h\nu + Lu^- \rightarrow Lu + e^-, \tag{4}$$

where Lu and Lu^- can be in excited states. The diagram labeled A in Fig. 2 is an energy level diagram of the first three states of neutral Lu. Overlaying this diagram to the spectrum shows that

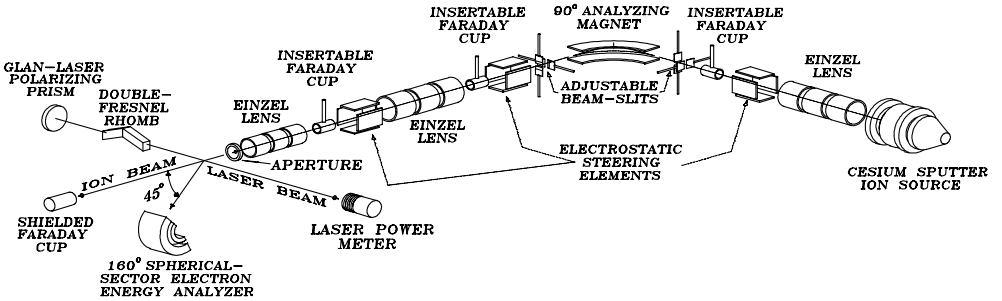

Fig. 1. Schematic of the LPES apparatus.

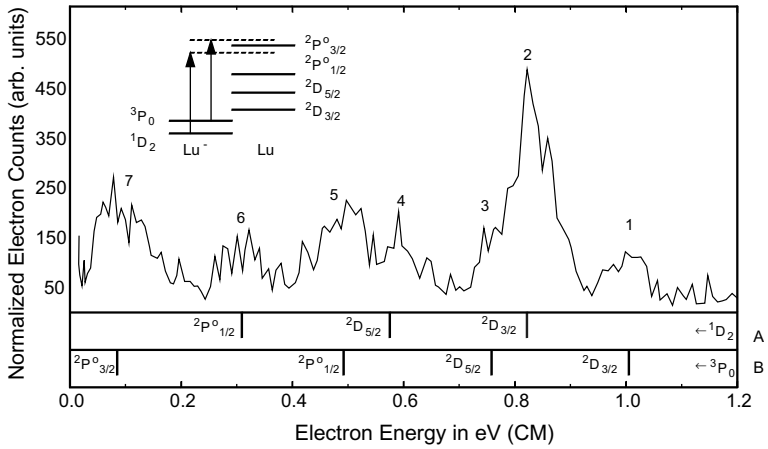

Fig. 2. Typical photoelectron kinetic energy spectrum for Photodetaching Lu^- Using a Nd:YAG laser [42]. The ion beam energy was 10 keV and the photon wavelength was 1064 nm (1.165 eV) for this spectrum. The inset in the upper left hand corner is a schematic of the energy level diagrams for Lu and Lu^-. The identification of the energy levels for Lu^- follows [16]. The peaks in the spectrum are labeled for further identification in the text. The energy level diagrams (labeled A and B) are discussed in the text.

the peaks in Fig. 2 labeled with even numbers represent transitions from the ground state of the negative ion, [Xe] ($4f^{14}6s^26p5d$) ($^1D_2$), to the first three states of neutral Lu. The diagram labeled B in Fig. 2 is also an energy level diagram of neutral lutetium, but is shifted from diagram A by the experimentally measured difference between the binding energies of the two states of Lu^-. Overlaying this diagram on the spectrum shows that the peaks in Fig. 2 labeled with odd numbers represent transitions from the excited state of the negative ion, [Xe] ($4f^{14}6s^26p^2$) ($^3P_0$), to the first four states of neutral Lu. Using this data, the electron affinity of Lu($^2D_{3/2}$) was determined to be $0.346 \pm$

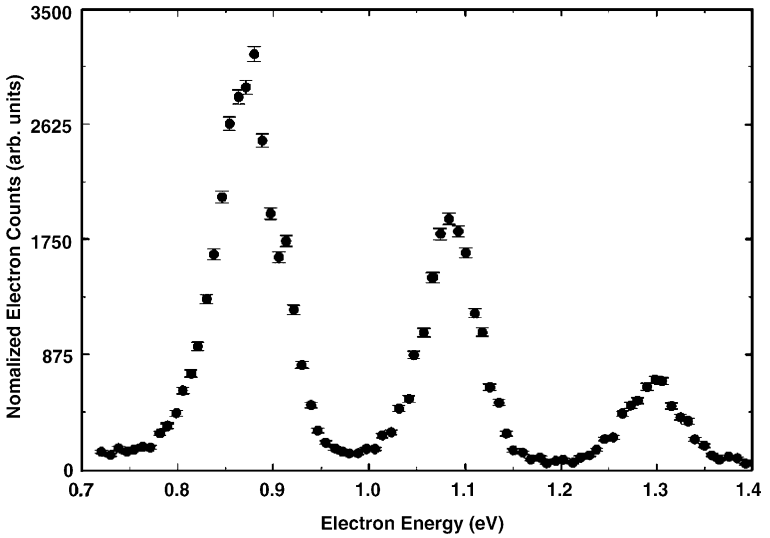

Fig. 3. Typical fine-structure-resolved photoelectron kinetic energy spectrum for photodetaching $Sn^-[h\nu + Sn^- \rightarrow Sn(^3P_{2,1,0}) + e^-]$. The ion-beam energy was 10 keV and the photon wavelength was 514.5 nm (2.410 eV) for this spectrum. The data points are plotted with error bars representing counting statistics at one standard deviation [27].

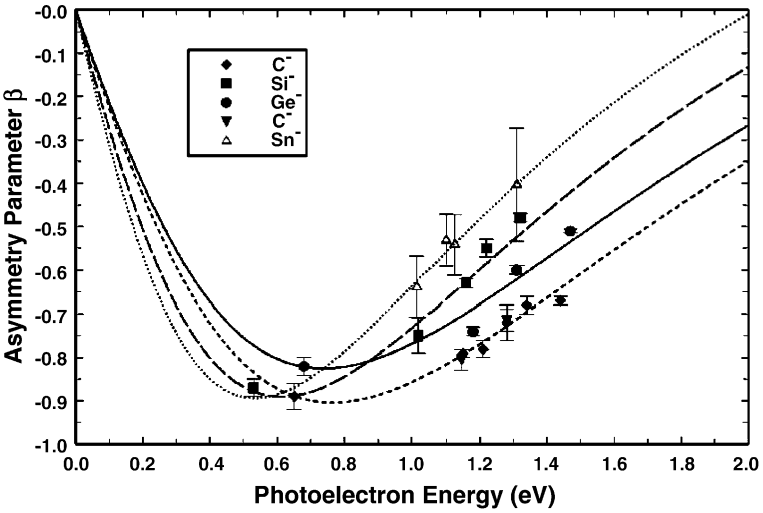

Fig. 4. Plot of photoelectron experimental asymmetry parameters versus photoelectron energy for C^- (diamonds, inverted triangles), Si^- (squares), Ge^- (circles), and Sn^- (open triangles) ([27, and references contained therein]). The lines are least-squares fits to a model of the spectral dependence of the asymmetry parameter ([25]). The short-dashed line is a fit to the asymmetry parameters for photodetaching C^-, the long-dashed line is a fit to the Si^- asymmetry parameters, the solid line is a fit to the Ge^- asymmetry parameters, and the dotted line is a fit to the Sn^- asymmetry parameters.

0.014 eV. The data also show that Lu^- has at least one bound excited state with a binding energy of 0.160 ± 0.020 eV relative to the ($^2D_{3/2}$) ground state of the neutral lutetium atom. EAs for several other lanthanides and hafnium were measured in a similar manner. The results are listed in Table 1.

The LPES method has also been used to study the photoelectron angular distributions of several heavy atomic anions. A typical photoelectron energy spectrum of Sn^- is shown in Fig. 3. The energy scale for the spectra was set using the known electron affinity of tin [30]. Details of the experiment and subsequent data analysis are given in [27]. A graph of the spectral dependence of the asymmetry parameters for several atomic anions for which a p-electron was detached is shown in Fig. 4. The quality of the fits using Eq. (3) to the C^-, Si^-, Ge^- and Sn^- asymmetry parameter data indicate that the assumptions made in the Cooper–Zare model and the subsequent simplification by Hanstorp et al. are valid for these ions over the photoelectron energy range investigated in this study, and demonstrate that the description of photoelectron angular distributions based on the independent-particle approximation is adequate for describing photodetachment processes for an ion as heavy as Sn^- [27].

References

[1] I.Yu. Kiyan, U. Berzinsh, J. Sandstrom, D. Hanstorp, Phys. Rev. Lett. 84 (2000) 5979.
[2] C. Blondel, Phys. Scr. T 58 (1995) 31.
[3] T. Andersen, Phys. Scr. T 34 (1991) 23.
[4] T. Andersen, H.K. Haugen, H. Hotop, J. Phys. Chem. Ref. Data 28 (1999) 1511.
[5] T. Andersen, Phys. Rpt. 394 (2004) 156.
[6] R.J. Zollweg, J. Chem. Phys. 50 (1969) 4251.
[7] B.M. Angelov, Chem. Phys. Lett. 43 (1976) 368.
[8] S.G. Bratch, Chem. Phys. Lett. 98 (1983) 113.
[9] S.H. Vosko, J.A. Chevary, I.L. Meyer, J. Phys. B 24 (1991) L225.
[10] S.H. Vosko, J.B. Lagowski, I.L. Mayer, J.A. Chevary, Phys. Rev. A 43 (1991) 6389.
[11] A.A. Griakina, G.F. Gribakin, V.K. Ivanov, Phys. Lett. A 168 (1992) 280.
[12] S.H. Vosko, J.A. Chevary, J. Phys. B 26 (1993) 873.
[13] D. Datta, D.R. Beck, Phys. Rev. A 47 (1993) 5198.
[14] K. Dinov, D.R. Beck, D. Datta, Phys. Rev. A 50 (1994) 1114.
[15] J.A. Chevary, S.H. Vosko, J. Phys. B 27 (1994) 657.
[16] E. Eliav, U. Kaldor, Y. Ishikawa, Phys. Rev. A 52 (1995) 291.

[17] S.M. O'Malley, D.R. Beck, Phys. Rev. A 61 (2000) 034501.
[18] S.M. O'Malley, D.R. Beck, Phys. Rev. A 70 (2004) 022502.
[19] X. Ciao, M. Dolg, Phys Rev. A 69 (2004) 042508.
[20] M.A. Garwan, A.E. Litherland, M.J. Nadeau, X.L. Zhao, Nucl. Instr. and Meth. B 79 (1993) 631.
[21] M.J. Nadeau, M.A. Garwan, X.L. Zhao, A.E. Litherland, Nucl. Instr. and Meth. B 123 (1997) 521.
[22] C.N. Yang, Phys. Rev. 74 (1948) 764.
[23] J. Cooper, R.N. Zare, in: S. Geltman, K.T. Mahanthappa, W.E. Britten (Eds.), Lectures in Theoretical Physics: Atomic Collision Processes, Vol. XI–C, Gordon and Breach, New York, 1969, p. 317.
[24] J. Cooper, R.N. Zare, J. Chem. Phys. 48 (1968) 942.
[25] D. Hanstorp, C. Bengstsson, D.J. Larson, Phys. Rev. A 40 (1989) 670.
[26] J.L. Hall, M.W. Siegel, J. Chem. Phys. 48 (1968) 943.
[27] V.T. Davis, J. Ashokkumar, J.S. Thompson, Phys. Rev. A 65 (2002) 024702.
[28] A.M. Covington, D. Calabrese, W.W. Williams, J.S. Thompson, T.J. Kvale, Phys. Rev. A 56 (1997) 1.
[29] W.C. Martin, R. Zalubas, L. Hagan (Eds.) Atomic Energy Levels, The Rare-Earth Elements (National Standard Reference Data Series-National Bureau of Standards 60), Washington DC, 1978.
[30] D.R. Lide (Ed.), CRC Handbook of Chemistry and Physics, CRC, Boca Raton, FL, 2000–2001.
[31] E. Eliav, A. Landau, U. Kaldor, Relativistic Coupled-Cluster Studies of Negative Ions, unpublished monograph.
[32] A.M. Covington, D. Calabrese, J.S. Thompson, T.J. Kvale, J. Phys. B 31 (1998) L855.
[33] V.T. Davis, J.S. Thompson, Phys. Rev. Lett. 88 (2002) 073003.
[34] D. Berkovits, S. Ghelberg, O. Herber, M. Paul, Nucl. Instr. and Meth. B 123 (1997) 515.
[35] V.T. Davis, J.S. Thompson, J. Phys. B 35 (2002) L11.
[36] K. Dinov, D.R. Beck, Phys. Rev. A 51 (1995) 1680.
[37] V.T. Davis, J.S. Thompson, J. Phys. B 37 (2004) 1961.
[38] V.T. Davis, J.S. Thompson, Phys. Rev. A 65 (2001) 010501.
[39] M.J. Nadeau, A.E. Litherland, M.A. Garwan, X.L. Zhao, Nucl. Instr. and Meth. B 92 (1994) 265.
[40] E.N. Avgoustoglou, D.R. Beck, Phys. Rev. A 55 (1997) 4143.
[41] H.H. Andersen, T. Andersen, U.V. Pedersen, Phys. Rev. B 31 (1998) 2239.
[42] V.T. Davis, J.S. Thompson, J. Phys. B. 34 (2001) L433.